Title

Rational Protein Design Yields a CD20 CAR with Superior Antitumor Efficacy Compared with CD19 CAR

Journal

Cancer Immunology Research, 11(2)

ISSN

2326-6066

Authors

Chen, Ximin
Chen, Laurence C
Khericha, Mobina
et al.

Publication Date

2023-02-03

DOI

10.1158/2326-6066.cir-22-0504

Peer reviewed

HHS Public Access

Author manuscript

Cancer Immunol Res. Author manuscript; available in PMC 2023 August 03.

Published in final edited form as:

Cancer Immunol Res. 2023 February 03; 11(2): 150–163. doi:10.1158/2326-6066.CIR-22-0504.

Rational protein design yields a CD20 CAR with superior antitumor efficacy compared to CD19 CAR

Ximin Chen[1,†], **Laurence C. Chen**[1,†], **Mobina Khericha**[1], **Xiangzhi Meng**[2], **Emma Salvestrini**[1], **Amanda Shafer**[2], **Neha Iyer**[3], **Anya S. Alag**[2], **Yunfeng Ding**[1], **Demetri M. Nicolaou**[1], **Yvonne Y. Chen**[1,2,4,*]

[1]Department of Chemical and Biomolecular Engineering, University of California, Los Angeles, Los Angeles, CA 90095, USA

[2]Department of Microbiology, Immunology, and Molecular Genetics, University of California, Los Angeles, Los Angeles, CA 90095, USA

[3]Department of Bioengineering, University of California, Los Angeles, CA 90095, USA

[4]Parker Institute for Cancer Immunotherapy Center at UCLA, Los Angeles, CA 90095, USA

Abstract

Chimeric antigen receptors (CARs) are fusion proteins whose functional domains are often connected in a plug-and-play manner to generate multiple CAR variants. However, CARs with highly similar sequences can exhibit dramatic differences in function. Thus, approaches to rationally optimize CAR proteins are critical to the development of effective CAR T-cell therapies. Here, we report that as few as two amino-acid changes in non-signaling domains of a CAR were able to significantly enhance *in vivo* antitumor efficacy. We demonstrate juxtamembrane alanine insertion and single-chain variable fragment (scFv) sequence hybridization as two strategies that could be combined to maximize CAR functionality, and describe a CD20 CAR that outperformed the CD19 CAR in antitumor efficacy in preclinical *in vitro* and *in vivo* assays. Precise changes in the CAR sequence drove dramatically different transcriptomic profiles upon antigen stimulation, with the most efficacious CAR inducing an enrichment in highly functional memory T cells upon antigen stimulation. These findings underscore the importance of sequence-level optimization to

[*]Corresponding author. yvchen@ucla.edu. Mailing address: 609 Charles E. Young Drive, East, 1602 Molecular Sciences Building, Los Angeles, CA 90095. Phone: 626-675-6596.
[†]These authors contributed equally to this work

AUTHOR CONTRIBUTIONS

- Conceptualization: YYC, XC, LCC
- Methodology: YYC, XC, LCC, XM
- Validation: XC, MK, YYC, LCC
- Formal analysis: XC, LCC, XM, YYC
- Investigation: XC, MK, LCC, ES, AS, NI, AA, YD, DN
- Writing—original draft: YYC, LCC
- Writing—review and editing: YYC, XC, LCC
- Supervision: YYC
- Funding acquisition: YYC

CAR T-cell function, and the protein-engineering strategy described here may be applied to the development of additional CARs against diverse antigens.

Keywords

Chimeric antigen receptor (CAR); T-cell therapy; protein engineering; immuno-oncology; synthetic biology

INTRODUCTION

The adoptive transfer of CD19-targeting chimeric antigen receptor (CAR) T cells has shown remarkable efficacy in treating advanced B-cell malignancies, but many patients receiving CD19 CAR T cells are unable to maintain long-term remission (1,2). One known cause for treatment failure or relapse after CD19 CAR T-cell therapy is tumor antigen escape (3–5). This impacts up to 94% of patients with B-cell acute lymphoblastic leukemia who relapse after CD19 CAR T-cell therapy (6–9). Antigen escape also impacts patients with refractory large B-cell lymphomas, with one trial reporting CD19 antigen loss in 27% of patients who experienced disease progression following treatment with axicabtagene ciloleucel, an FDA-approved CD19 CAR T-cell product with a CD28 co-stimulatory domain in the CAR (10). CAR T cells that can respond to multiple B-cell antigens (e.g., CD19, CD20, and CD22) through bispecific or trispecific CAR architectures can significantly lower the risk of tumor escape by CD19 antigen loss (11–13). However, such strategies come at the cost of increasing genetic payload size, which decreases the transduction efficiency and fraction of CAR-expressing T cells in the manufactured patient product (14,15). Moreover, tumors can downregulate both CD19 and CD22 in response to immunotherapy (16). In contrast, clinical evidence suggests CD20 may be more resistant to antigen escape than CD19, even under selective pressure from immunotherapy (12,17). Yet, CD20-targeting CAR T cells have shown uneven clinical responses to date (18–21). Several ongoing trials suggest early signs of promise with newer-generation CD20 CAR T cells (22–24), but none has yet shown clear superiority over CD19 CAR T–cell therapy. Therefore, the development of a robust CD20 CAR, particularly one that can outperform CD19 CAR T cells in the context of lymphoma, would be of strong translational value.

Here, we used rational protein design to alter residues in between and within functional CAR domains to expand the CAR sequence search space. We generated CD20 CAR variants in which minute changes in CAR protein residues were observed to greatly alter CAR T–cell effector function, leading to significant improvements in *in vivo* antitumor efficacy when compared with the FMC63 scFv-based CD19 CAR and Leu16 scFv-based CD20 CAR in a lymphoma xenograft model. Newly engineered CD20 CAR variants enhanced *in vivo* tumor-killing efficacy by programming T cells to effectively transition from their resting state to a productively stimulated state, characterized by enrichment of highly functional memory T cells upon antigen exposure. Our findings demonstrate the importance of precise rational protein design in maximizing CAR T–cell function, yielding a CD20 CAR that outperforms clinical benchmarks and has strong translational potential.

MATERIALS AND METHODS

Construction of anti-CD20 scFvs and CARs

Plasmids encoding scFv sequences of rituximab were generous gifts from Dr. Anna M. Wu (UCLA and City of Hope) (25). Plasmid encoding scFv derived from the leu16 monoclonal antibody (mAb) was a generous gift from Dr. Michael C. Jensen (Seattle Children's Research Institute) (24). The sequence of the anti-GD2 14g2a scFv was obtained from protein data bank (PDB: 4TUJ). CD19 scFv was derived from FMC63 mAb (26). All constructs were cloned into the MSCV retroviral expression vector (27,28). The MSCV-IRES-EGFP retroviral vector and retroviral packaging vectors, pHIT60 and RD114, were generous gifts from Dr. Owen Witte (UCLA), who received the original backbone from Dr. Steven Feldman (National Cancer Institute). A Woodchuck hepatitis virus posttranscriptional regulatory element (WPRE) was inserted in the ClaI site behind the EGFP transgene to generate the MSCV-IRES-EGFP-WPRE vector that was used in subsequent cloning of all MSCV-based constructs (29). CD20 CARs and the GD2 CAR were constructed by assembling an scFv (in V_L–V_H orientation for CD20 CARs, and in V_H–V_L orientation for GD2 CAR), an extracellular IgG4 hinge–CH2–CH3 spacer containing the L235E N297Q mutation (30), the CD28 transmembrane and cytoplasmic domains, the CD3ζ cytoplasmic domain, and a T2A "self-cleaving" sequence followed by a truncated epidermal growth factor receptor (EGFRt). CD19 CAR was constructed by assembling an scFv (in V_L–V_H orientation), an extracellular IgG4 hinge, the CD28 transmembrane and cytoplasmic domains, the CD3ζ cytoplasmic domain, and a T2A "self-cleaving" sequence followed by a truncated epidermal growth factor receptor (EGFRt). EGFRt was used as a surrogate marker for CAR transduction efficiency and also facilitated sorting of CAR^+ T cells. The CAR-T2A-EGFRt sequence was cloned downstream of the 5' LTR in the MSCV vector in lieu of the IRES-EGFP sequence. The EGFP-HaloTag 2 sequence was PCR amplified from a HA-EGFP-HaloTag2 epHIV7 plasmid (Addgene #41742). The EGFP-HaloTag2 sequence was incorporated downstream of CD19 or CD20 CAR sequences from the abovementioned CD20 CAR constructs into the epHIV7 vector (13) in order to generate CAR–HaloTag fusion proteins for microscopy imaging of CAR clustering (31). DNA sequences encoding for one to four alanine residues were inserted between CD28 transmembrane and cytoplasmic domain via isothermal assembly in our rituximab-based CD20 CAR and our 14g2a-based GD2-targeting CAR studies. Both hybrid CD20 CAR sequences were synthesized as gene block fragments (by Integrated DNA Technologies, IDT) and assembled into the rituximab-based CD20 CAR-T2A-EGFRt in MSCV backbone via digestion-ligation with MreI and BstBI.

Cell line generation and maintenance

Jurkat (Clone E6-1) and HEK293T cells were obtained from ATCC in 2011. These cell lines have not been independently authenticated beyond certification by ATCC. HEK293T cells were cultured in DMEM (HyClone #SH30243.01) supplemented with 10% heat-inactivated FBS (HI-FBS; ThermoFisher #10082147). Raji and K562 cells were cultured in RPMI-1640 (Lonza #BE04-558F) with 10% HI-FBS. Leu16, Rituximab and RFR-LCDR (hybrid) scFv-expressing HEK293T cell lines were generated by retroviral transduction of HEK293T cells to express each scFv fused with EGFP via a 2A peptide. In brief, 2 mL retroviral supernatant

(see Retrovirus production and generation of human primary CAR T cells) with 4 μg/mL of polybrene was added to 1 x 10^6 HEK293T cells and incubated at 37 °C with 5% CO_2 for 48 hours. Afterwards, retroviral supernatant was removed and transduced HEK293T cells were expanded for ten days using fresh complete media. $EGFP^+$ cells were sorted by fluorescence-activated cell sorting (FACS) on a FACSAria (II) cell sorter (BD Bioscience) at the UCLA Flow Cytometry Core Facility to enrich for the scFv-expressing population. K562 cells and Raji cells expressing EGFP and firefly luciferase (ffLuc) were gifts from Dr. Michael C. Jensen (Seattle Children's Research Institute) in 2011. Dr. Jensen originally obtained the parental Raji cells from ATCC in 2003, and received the parental K562 cells as a gift from Dr. Laurence Cooper in 2001. Both lines were authenticated by short tandem repeat profiling at the University of Arizona Genetics Core in 2015. $CD20^+$ K562 cells were generated by transduction of K562 cells with a retroviral construct encoding full-length CD20 (Uniprot P11836). $CD20^+$ K562 cells were stained with an anti-CD20 antibody (PE, Clone 2H7, BioLegend #302346) and were sorted by FACS into bins of different CD20 antigen densities to generate $CD20^{hi}$, $CD20^{med}$, $CD20^{low}$ K562 cell lines. Jurkat cells were lentivirally transduced to express CD19 or CD20 CARs directly fused to EGFP-HaloTag for microscopy experiments. Lentivirus was produced using HEK293T cells as previously described (13). Cell lines used for *in vitro* and *in vivo* experiments were cultured with a maximum of twenty and ten passages, respectively. All cell cultures were tested for mycoplasma on a monthly basis and confirmed to be mycoplasma negative.

Retrovirus production and generation of human primary CAR T cells

Retroviral supernatants were produced by transient co-transfection of HEK293T cells with pRD114/pHIT60 virus-packaging plasmids (gifts from Dr. Steven Feldman of National Cancer Institute) and plasmids encoding CARs or control constructs using linear polyethylenimine (PEI, 25 kDa; Polysciences #23966-1). Supernatants were collected 48 and 72 hours later and pooled after removal of cell debris using a 0.45 μm membrane filter. Healthy donor blood was obtained from the UCLA Blood and Platelet Center. $CD8^+$ T cells were isolated using RosetteSep Human $CD8^+$ T Cell Enrichment Cocktail (StemCell Technologies #15063) according to the manufacturer's protocol. Peripheral blood mononuclear cells (PBMCs) were isolated from a Ficoll-Paque PLUS (GE Healthcare #GE17-1440-02) density gradient. $CD14^-CD25^-CD62L^+$ naïve/memory T cells ($T_{N/M}$) were enriched from PBMCs using magnetic-activated cell sorting (MACS; Miltenyi) as previously described (32). In brief, PBMCs were labeled with anti-CD14 (Miltenyi #130-050-201) and anti-CD25 microbeads (Miltenyi #130-092-983) to deplete $CD14^+$ and $CD25^+$ cells. The negative population was subsequently labeled with anti-CD62L microbeads (Miltenyi #130-091-758) to enrich for $CD14^-CD25^-CD62L^+$ naïve/memory T cells ($T_{N/M}$). $CD8^+$ T cells were used in early experiments. $T_{N/M}$ cells, which have more recently been shown to exhibit clinical potential as a highly functional starting population for therapeutic T-cell manufacturing (NCT04007029), were used in subsequent *in vitro* and *in vivo* studies. Both $CD8^+$ T cells and $T_{N/M}$ cells were stimulated with CD3/CD28 Dynabeads (ThermoFisher #11132D) at a 3:1 cell-to-bead ratio on Day 0 (day of isolation) and transduced with retroviral supernatant on Day 2 and Day 3. Dynabeads were removed on Day 7. T cells were cultured in T-cell media (RPMI-1640 supplemented with 10% HI-FBS) and fed with recombinant human IL2 (ThermoFisher #PHC0023) and IL15 (Miltenyi

#130-095-765) every 2 days to final concentrations of 50 U/mL and 1 ng/mL, respectively. For CAR T cells used in RNA-seq and ATAC-seq experiments, T cells were enriched for CAR^+ expression by magnetic cell sorting via staining of EGFRt with biotinylated cetuximab (Eli Lilly; biotinylated in-house) followed by anti-biotin microbeads (Miltenyi #130-090-485). For RNA-seq and ATAC-seq, dead cells were depleted with a dead cell removal kit (Miltenyi #130-090-101) prior to enrichment of $EGFRt^+$ population.

Cytotoxicity assay with repeated antigen challenge

CAR^+ T cells were seeded at 4 x 10^5 cells/well in 24-well plates and coincubated with or without K562 (parental and CD20-expressing) target cells at a 2:1 E:T ratio. Untransduced T cells were added to wells as needed to normalize for differing transduction efficiencies and ensure the total number of T cells per well was consistent throughout. Cell counts were quantified using a MACSQuant VYB flow cytometer every 2 days prior to addition of fresh target cells (2 x 10^5 cells/well); cell count data were analyzed using the FlowJo software Version 10.4.0 (TreeStar).

Cytotoxicity assay with K562 target cells with varying CD20 expression levels

Four K562 cell lines (parental/$CD20^{neg}$, $CD20^{low}$, $CD20^{med}$, and $CD20^{hi}$) and Raji target cells were seeded at 1 x 10^5 cells/well in 96-well U-bottom plates. CAR^+ T cells were added to target cells at 0.1:1, 0.5:1 and 2:1 E:T ratios. Percent CAR^+ across each sample was normalized by supplementing untransduced T cells. Remaining target cells were quantified by MACSQuant VYB flow cytometer 24-hr post co-incubation.

Cytokine production quantification by ELISA

In 96-well U-bottom plates, 5 x 10^5 CAR^+ T cells were incubated with 2.5 x 10^5 EGFP-expressing parental K562 ($CD19^-CD20^-$) or $CD19^+CD20^+$ K562 target cells at a 2:1 effector-to-target (E:T) ratio. To control for cell density while accounting for differences in transduction efficiency, untransduced T cells were added as necessary to reach the same number of total T cells per well. After a 48-hour co-incubation, cells were spun down at 300 x g for 2 min. Supernatant was harvested and IL2, TNFα and IFNγ were quantified by ELISA MAX™ Standard Set (BioLegend# 431804, #430204, #430101).

Proliferation assay

T cells were stained with 1.25 μM CellTrace Violet (ThermoFisher #C34557) and 4 x 10^5 CAR^+ T cells were seeded in each well in 96-well U-bottom plates with $CD19^+CD20^+$ K562 cells at a 2:1 E:T ratio. Untransduced T cells were added to wells as needed to normalize for differing transduction efficiencies and ensure the total number of T cells per well was consistent throughout. Cultures were passaged as needed, and CTV dilution was analyzed on a MACSQuant VYB flow cytometer after a 4-day co-incubation.

Western Blots

Twenty million CAR^+ T cells were cultured with 0.02 mg/mL tunicamycin (Sigma #T7765-1MG) for 24 hours prior to cell lysis with RIPA buffer supplemented with protease inhibitor cocktail (Thermo Fisher Scientific #A32963). Cells were lysed for 30 min at 4°C

with gentle shaking. Lysates were centrifuged at 10,000 xg at 4°C to remove particulate matter prior to protein quantification using Bradford assay (Bio-Rad #5000201).

Whole-cell lysates (30–60 μg in 15 μL) mixed with 5 μL bolt LDS sample buffer (Thermo Fisher Scientific #B0007) were boiled at 70°C for 10 minutes. Twenty microliters of boiled lysates were loaded into 4–12% NuPAGE Bis-Tris gels (Thermo Fisher Scientific #NP0321BOX) and transferred onto nitrocellulose membranes using the iBlot gel transfer system (Thermo Fisher Scientific). Membranes were blocked with 5% bovine serum albumin (BSA) in 1X TBS-T (50 mM Tris, 150 mM NaCl, 0.05% Tween 20, pH = 7.8) for 45 minutes and stained with anti-CD3ζ (clone 8D3, BD Biosciences #551304, 1:500 dilution) for 1 hour, followed by staining with anti-mouse IgG (H+L)-HRP (polyclonal, Jackson ImmunoResearch #115-035-003) for 1 hour. Membranes were incubated in SuperSignal West Dura Extended Substrate (Thermo Fisher Scientific #34075) for 30 seconds and imaged using ChemiDoc Touch Imaging System (Bio-Rad).

Antibody staining for flow-cytometry analysis

EGFRt expression was measured with biotinylated cetuximab (Eli Lilly; biotinylated in-house), followed by PE-conjugated streptavidin (Jackson ImmunoResearch #016-110-084). CAR expression was quantified by surface epitope staining using anti-Fc (Alexa Fluor 488, Jackson ImmunoResearch #709-546-098). CD20 expression levels on target cells were evaluated by staining for CD20 (PE, clone 2H7, BioLegend #302346). T-cell subtypes were evaluated by staining with anti-CD45RA (FITC, clone HI100, BioLegend #304148, anti-CD62L (eFluor450, clone DREG-56, Thermo Fisher #48-0629-42). T-cell persistence *in vivo* was monitored by antibody staining of retro-orbital blood samples. Samples were treated with red blood cell lysis solution (10X, Miltenyi #130-094-183) following the manufacturer's protocol. The remaining cellular content was stained with anti-human CD45 (PacBlue or PECy7, clone HI30, BioLegend #304029 or #304016) and biotinylated cetuximab, followed by PE-conjugated streptavidin. *In vivo* T-cell phenotypes were measured by staining using anti–PD-1 (PE-Vio770, Clone REA1165, Miltenyi #130-120-385), anti–LAG-3 (APC, Clone 7H2C65, BioLegend #369212), anti–CTLA-4 (APC, Clone BNI3, BioLegend #369612), and anti–CD137 (PE/Cy7, Clone 4B4-1, BioLegend #309818) and analyzed among the $CD45^{+}EGFRt^{+}$ population. All samples were analyzed on a MACSQuant VYB flow cytometer (Miltenyi), and the resulting data were analyzed using the FlowJo software Version 10.4.0 (TreeStar).

Confocal microscopy

Imaging experiments were done using CAR-expressing Jurkat cells stained with anti-Fc antibody conjugated to DyLight 405 (Jackson ImmunoResearch #109-477-008), and with Jurkat cells transduced with CAR–HaloTag fusion protein stained with the red fluorescent dye tetramethylrhodamine (TMR) ligand (Promega #G8251) following manufacturer's protocol. In both experiments, CAR-expressing Jurkat cells were seeded at 1×10^5 cells per well in 50 μL RPMI-1640 + 10% HI-FBS in one well of a 48-well flat-bottom glass plate (MatTek) without antigen stimulation. Scanning confocal imaging was acquired with a Zeiss LSM 880 laser scanning confocal microscope with AiryScan and a 63X 1.4 NA oil objective.

Bio-layer interferometry (BLI) analysis of binding kinetics

Biotinylated peptide including the CD20 epitope (INIYNCEPANPSEKNSPSTQYCYSIQS) was synthesized by GenScript (Piscataway, NJ). Binding interaction between Leu16, Rituximab and Hybrid (RFR–LCR) scFv (Analyte) and the CD20 epitope was quantified by bio-layer interferometry performed on an Octet RED system (ForteBio Octet RED96e). All interaction studies were performed with Streptavidin (SA) dip and read biosensors (ForteBio), with assays conducted at 25°C in MOPS Buffer (20mM MOPS pH 8.0, 50mM KCl, 0.5mg/mL BSA). Leu16, Rituximab and Hybrid scFv with N-terminal polyhistidine tag (6X-His) were purified from HEK293T supernatant using Ni-NTA beads (Genesee #20-512) and quantified by Bradford assay. Biotinylated CD20 peptide was loaded onto SA biosensors for 180 seconds. Two hundred microliters of sample or buffer were used in 96-well flat-bottom microplates (Greiner) and agitated at 800 x g. The loaded biosensors were washed in buffer for 60 seconds and transferred to the wells containing analyte at various concentrations in buffer. Association between the analyte and ligand was observed for 300 seconds, and dissociation was subsequently observed for 300 seconds, for each analyte in MOPS Buffer. Kinetic parameters (k_{on} and k_{off}) and binding affinity (K_D) were calculated from a non-linear global fit of the data between the analyte and ligand using the Octet software (Data Analysis HT 11.1.3.50). Independent measurements were performed three times for each scFv, using fresh biosensors and fresh protein dilutions each time.

In vivo studies

All animal studies were performed in accordance with and with the approval of the UCLA Institutional Animal Care and Used Committee. Six- to eight-week-old NOD/SCID/IL-2Rγ^{null} (NSG) mice were obtained from UCLA Department of Radiation and Oncology. Mice were injected with 0.5 x 10^6 $EGFP^+$ $ffLuc^+$ Raji lymphoma cells by tail-vein injection, randomized into treatment groups based on radiance levels, and subsequently treated with CAR T cells or cells expressing EGFRt only (negative control) via tail-vein injection. Details of the dose and timing of tumor injection, T-cell injection, and tumor re-challenge are indicated in the text and figures. Tumor progression/regression was monitored with an IVIS Illumina III LT Imaging System (PerkinElmer). Blood samples were harvested via retro-orbital bleeding 3 days post T-cell injection and every 10–13 days thereafter. Mice were closely monitored for signs of sickness and euthanized at the humane endpoint, defined as the point when a mouse was unable to rise, reach food, or move in a desired direction, had noticeable respiratory effort, was unable to recover from a dorsal position, showed signs of paralysis, or experienced more than 10% weight loss. Bone marrow, spleen and liver were collected after euthanasia. Tissues were ground and passed through a 100-μm filter followed by red-blood-cell lysis prior to flow-cytometry analysis. Studies aimed at collecting survival data were blinded to the operator. For ATAC-seq and RNA-seq experiments, NSG mice were engrafted with 0.5 x 10^6 Raji cells 6 days prior to treatment with 2.85 x 10^6 CAR T cells. Nine days after T-cell injection, CAR T cells were recovered from animal tissues (liver, spleen, cardiac blood, and bone marrow) and enriched for the $huCD45^+EGFRt^+$ subpopulation by MACS prior to ATAC-seq and RNA-seq library construction. In brief, organs were ground and passed through a 100-μm filter into single-cell suspension (different organs from the same mouse were combined for analysis). Red-blood-cell lysis was performed. Cells were stained with anti-huCD45 antibody (BioLegend, PE, Clone HI30,

#304039) followed by anti-PE microbeads labeling (Miltenyi #130-048-801). Labeled cells were passed through MS columns (Miltenyi #130-042-201) on an OctoMACS Saparator (Miltenyi #130-042-108). The positive fractions were collected for ATAC-Seq and RNA-seq library construction.

ATAC-seq library construction and data analysis

ATAC-seq libraries were constructed as previously described (33,34). In brief, 30,000–50,000 viable huCD45$^+$EGFRt$^+$ human CAR T cells per mouse, obtained by MACS (see In vivo studies), were washed once with PBS and lysed in 50 μL Resuspension Buffer (RSB) buffer (10 mM Tris-HCL, pH 7.4, 10 mM NaCl, 3 mM $MgCl_2$) with 0.1% IGEPAL CA-630, 0.1% Tween-20, and 0.01% digitonin. Samples were washed with 1 mL RSB buffer containing 0.1% Tween-20 and centrifuged at 500 x g for 10 minutes at 4°C. Pelleted nuclei were resuspended in 25 μL Tn5 transposition mix (12.5 μL 2X Tagment DNA buffer, 1.25 μL Tn5 transposase, and 11.25 μL sterile water; Illumina #20034197) and stored in a shaking incubator at 37°C and 500 RPM for one hour. Transposition reaction was purified with DNA Clean & Concentrator kit (Zymo Research #D4004). DNA fragments were PCR-amplified using NEB Q5 MasterMix (New England BioLabs #M0492L) and custom primers as previously described (33). Libraries were size selected by AmPure beads (Beckman Coulter #A63881) and quantified by TapeStation. Libraries were sequenced on the Illumina NovaSeq S1 platform at the High Throughput Sequencing core at UCLA Broad Stem Cell Research Center with 50-bp paired-end reads. Fastq files from ATAC-seq were quality examined by FastQC (Linux, v0.11.8). Reads were processed by cutadapt (Linux, v1.18) to remove reads with low quality (quality score < 33) and to trim adapters. Trimmed reads were aligned to mm10 reference genome using Bowtie2 (Linux, v2.2.9) to eliminate contaminating reads from mouse cells. Non-murine reads were subsequently mapped to hg38 genome by Bowtie2, and sam files were converted to bam files by samtools (Linux, v1.9). Peaks were called independently for each replicate using MACS2 (Linux, v2.1.2) on the aligned reads, and subsequently merged by bedtools (v2.26.0). Fragments assigned to each peak were counted by f*eatureCounts* function in subread (Linux, v1.6.3). To visualize chromatin accessible sites, peaks called from MACS2 were visualized in IGV (v2.8.0). Fold enrichments (calculated by MACS2) of peaks within −1 kb to 1 kb of the transcription start site (TSS) indicate accessibility of promoter regions.

Bulk RNA-seq for CAR T cells recovered from tumor-bearing mice

Total RNA was extracted from 200,000–700,000 MACS-sorted CAR T cells using Qiagen RNeasy Plus Mini kit (Qiagen #74104). mRNAs were isolated using NEBNext Poly(A) mRNA Magnetic Isolation Module (New England BioLabs #E7490L). RNA-seq libraries were generated using NEBNext Ultra II Directional RNA Library Prep Kit (New England BioLabs #E7760L) following the manufacturer's protocol. Libraries were sequenced on the Illumina NovaSeq S1 platform at the High Throughput Sequencing core at UCLA Broad Stem Cell Research Center with 50-bp paired-end reads. Fastq files from RNA-seq were quality-examined by FastQC (Linux, v0.11.8). Reads were processed by cutadapt (Linux, v1.18) to remove reads with low quality (quality score < 33) and to trim adapters. Trimmed reads were aligned to mm10 reference genome using Tophat2 (Linux, v2.1.0) to remove the contaminated reads from mouse cells. Non-murine reads were mapped to hg38 genome by

Tophat2. Reads assigned to each gene were counted by *featureCounts* function in subread package (Linux, v1.6.3) with Ensembl 38 gene sets as references. Genes without at least 8 reads mapped in at least one sample were considered below reliable detection limit and eliminated. Read counts were normalized by Trimmed Mean of M-values method (TMM normalization method in edgeR running on R v3.6.3) to yield FPKM (fragments per millions per kilobases) values, and differential expression was calculated using the package edgeR.

Bulk RNA-seq for CAR T cells cultured *ex vivo*

$CD14^{-}CD25^{-}CD62L^{+}$ naïve/memory T cells ($T_{N/M}$) were isolated, activated, retrovirally transduced as described above (see Retrovirus production and generation of human primary CAR T cells). On day 16 or 18 post activation, total RNA was extracted from MACS-sorted CAR T cells using Qiagen RNeasy Plus Mini kit (Qiagen #74104). mRNAs were isolated using NEBNext Poly(A) mRNA Magnetic Isolation Module (New England BioLabs #E7490L). RNA-seq libraries were generated using NEBNext Ultra II Directional RNA Library Prep Kit (New England BioLabs #E7760L) following the manufacturer's protocol. Libraries were sequenced on the Illumina NovaSeq S1 platform at the High Throughput Sequencing core at UCLA Broad Stem Cell Research Center with 50-bp paired-end reads. Fastq files from RNA-seq were quality-examined by FastQC (Linux, v0.11.8). Reads were processed by cutadapt (Linux, v1.18) to remove reads with low quality (quality score < 33) and to trim adapters. Trimmed reads were mapped to hg38 genome by Tophat2. Fragments assigned to each gene were counted by *featureCounts* function in subread package (Linux, v1.6.3) with Ensembl 38 gene sets as references. Genes without at least 8 reads mapped in at least one sample were considered below reliable detection limit and eliminated. Read counts were normalized by Trimmed Mean of M-values method (TMM normalization method in edgeR running on R v3.6.3) to yield FPKM (fragments per millions per kilobases) values.

Gene set enrichment analysis (GSEA) and Enrichr analysis

GO analysis was performed using GSEA software (v4.1.0, Broad Institute) and BubbleGUM (v1.3.19) (35). Expression values of differentially expressed genes were input to the program and using a curated list of 2,493 T cell–relevant gene sets selected from current Molecular Signatures Database (MsigDB) gene sets (Supplementary Data S1). Differentially expressed genes were used to perform GO Biological Process (2021 version), GO Molecular Function (2021 version), Kyoto Encyclopedia of Genes and Genomes (KEGG; 2021 version), and MsigDB Hallmark (2020 version) pathway enrichment using Enrichr (36). Top 10 pathways with adjusted *p* value that were less than 0.05 and were related to T-cell signaling, effector function and metabolism from were chosen to display. Heatmaps for differentially expressed genes were generated using *heatmap.plus, pheatmap* and *ggplot2* packages in R (version 3.6.3). Volcano plots were generated using *ggplot2* in R (version 3.6.3).

Statistical Analysis

Statistical tests including two-tailed, unpaired, two-sample Student's *t* test with Sidak correction for multiple comparisons and log-rank Mentel-Cox test with Holm-Sidak correction for multiple comparisons were performed using GraphPad Prism V8. One-way ANOVA test for differential gene analysis in RNA-seq was performed with *glmQLFTest*

function in edgeR. Fisher's exact test and the Benjamini-Hochberg method were used to calculate *p* values and adjusted *p* values, respectively, in Enrichr.

Data Availability Statement

The data generated in this study, including RNA-seq and ATAC-seq data, are available within the article and its supplementary data files or from the corresponding author upon reasonable request.

RESULTS

Rituximab-based CD20 CAR T cells have limited antitumor efficacy

We began our engineering effort with a CD20 CAR containing a rituximab-based scFv and CD28 costimulatory domain (Fig. 1A). Rituximab, a CD20-specific mAb, is the front-line treatment option for a variety of B-cell malignancies (37). Since CD19 and CD20 are both present on B-cell lymphomas, the choice of CD20 as the target antigen allows direct comparison of a rituximab-based CAR and the FMC63-based CD19 CAR. All FDA-approved CD19 CARs contain the FMC63 scFv as the ligand-binding domain, and the CD19 CAR construct used in lisocabtagene maraleucel was used as a positive control throughout this study. The CD19 and CD20 CARs contain identical transmembrane and signaling domains, but were given different extracellular spacer lengths based on prior studies indicating different structural requirements for optimal CD19 and CD20 antigen targeting (13,38) (Fig. 1A). Specifically, it has been demonstrated that CD19 CARs containing a short (IgG4 hinge only) spacer are superior to otherwise identical CD19 CARs containing a long (IgG4 hinge-CH2-CH3) spacer (38). In contrast, robust CD20 CAR T–cell function requires incorporation of a long extracellular spacer (13). The long spacer used in this study contains two mutations (L235E N297Q) within the CH2 domain of IgG4 to reduce binding to soluble Fc-gamma receptors (39). Each CAR was connected via a self-cleaving T2A peptide to EGFRt as transduction marker; T cells transduced with EGFRt alone served as negative controls throughout this study. The rituximab-based CD20 CAR expressed on the surface of primary human T cells (Fig. 1B,C). However, we found that compared with the FMC63-based CD19 CAR, the CD20 CAR showed reduced tumor lysis and T-cell proliferation upon repeated antigen challenge (Fig. 1D).

Prior studies have suggested CAR clustering mediated by scFv aggregation at the cell surface as a cause of tonic signaling and T-cell dysfunction (40,41). We thus examined the CAR expression pattern as a potential cause of the suboptimal activity of the rituximab-based CD20 CAR. However, confocal microscopy revealed even distribution of the CD20 CAR on the T-cell surface, similar to the FMC63-based CD19 CAR (Fig. 1E,F). Furthermore, both FMC63 and rituximab are high-affinity binders of their respective antigens (26,42).Taken together, these results suggest factors beyond CAR protein distribution and external engagement with the antigen could be involved in the inability of the CD20 CAR to achieve robust activity, prompting us to examine the intracellular domains of the CARs and explore their impact on CAR T–cell function.

Insertion of torsional linkers improves rituximab-based CD20 CAR T–cell function

The CD19 and CD20 CARs evaluated in this work contain CD28 and CD3ζ signaling domains, whose downstream signaling cascades are mediated by adaptor proteins and kinases whose interactions depend on the protein conformation and physical accessibility of receptor chains (43). Receptor protein conformation is, in turn, a function of the overall protein sequence, not just domains that directly engage in ligand binding or signaling. We thus contemplated the possibility that different CARs containing the same signaling domains could exhibit different signaling behavior due to differences in overall protein conformation. Specifically, we hypothesized that differences in the conformation of the intracellular portion of a CAR could alter the accessibility of the receptor's docking residues to downstream signaling molecules, thus impacting the quality of the CAR's signaling.

CARs typically contain an α-helical transmembrane domain, such as the CD28 transmembrane domain used in the rituximab CAR (44). Alanine insertion is a well-established method to form or extend α-helices, with each alanine expected to cause an ~109° turn in the protein structure (45–47). For example, EAAAK is a frequently used rigid linker due to its stable α-helical conformation (32,48). We thus hypothesized that inserting alanine residues immediately after the transmembrane domain of a CAR would alter the receptor's conformation by extending the transmembrane helix, changing the accessibility of intracellular signaling domains to downstream signaling molecules. We further hypothesized that this could provide a means to calibrate CAR signaling without directly altering signaling domains of the CAR. A panel of receptors containing 0–4 alanine residues in the juxtamembrane position (i.e., between the transmembrane and cytoplasmic domains) was generated to allow varying alignments between the extracellular transmembrane domain and cytoplasmic signaling domains of each CAR (Fig. 2A; Supplementary Fig. S1A).

All alanine-insertion variants expressed on the T-cell surface, with no correlation between the number of alanines inserted and the level of CAR expressed on the surface (Supplementary Fig. S1B,C). Alanine-insertion variants showed comparable lysis and proliferation upon repeated stimulation with Raji cells *in vitro* compared to the parental (no-alanine) rituximab CAR T cells (Supplementary Fig. S1D). Across the alanine-insertion CAR constructs, no dramatic difference in antigen-dependent T-cell proliferation nor consistent trend in antigen-dependent cytokine production was observed in response to $CD20^+$ K562 target cells (Supplementary Fig. S1E,F), indicating a lack of observable differences in CAR T–cell function *in vitro*. However, the fact that CARs with clearly different antitumor efficacy *in vivo* can have indistinguishable or contradictory *in vitro* activity has previously been observed by our group and others (32,38,49), potentially because *in vivo* antitumor efficacy reflects the cumulative effects of *in vivo* expansion/persistence, cytokine production, and lytic capacity in a physiological context. To fully examine the effects of alanine insertion on CAR T–cell function, we proceeded with *in vivo* assessment in a Raji lymphoma xenograft model.

T cells expressing rituximab-based CARs containing 1 or 4 inserted alanines showed substantially improved *in vivo* tumor control compared to parental rituximab CAR T cells, whereas 3-alanine insertion provided no benefit (Fig. 2B). However, the 2-alanine insertion CAR significantly improved *in* vivo tumor control and increased median survival period by

2.1-fold compared to the original rituximab CAR (55 days vs. 26 days; Fig. 2C), indicating a small change in CAR protein sequence—at a position not directly involved in ligand binding or signaling—can exert significant impact on CAR T–cell function.

In principle, the insertion of alanine-based torsional linkers can be performed on any CAR protein, irrespective of the particular ligand-binding or signaling domains incorporated in the CAR. To probe the generalizability of this CAR-tuning method, we evaluated the effects of alanine insertion in the 14g2a-based GD2-targeting CAR, which is known to exhibit tonic signaling and premature exhaustion (50). All GD2 CAR variants expressed well on the T-cell surface (Supplementary Fig. S2A,B). In a neuroblastoma xenograft model, T cells expressing GD2 CARs containing 1, 2, or 4 inserted alanines improved tumor control compared to the parental GD2 CAR, whereas 3-alanine insertion again had no effect (Supplementary Fig. S2C), corroborating results from the CD20 CAR panel. Insertion of 1 alanine resulted in a statistically significant increase in survival (Supplementary Fig. S2D), while the 2-alanine CAR construct yielded the highest level of persisting T cells (Supplementary Fig. S2E).

The alanine-insertion strategy was devised based on the hypothesis that adding alanine residues would result in predictable “twisting” of the CAR protein conformation. Although structural confirmation is challenging due to the transmembrane nature of the CAR, the proposition that receptor function was altered through rotation of the CAR’s intracellular domain around a central axis—as opposed to simple elongation of the CAR—is consistent with the non-linear relationship between the number of alanines inserted and the antitumor efficacy observed in the lymphoma *in vivo* model. Further, the variant with 3 alanines inserted is expected to experience a ~327° rotation, which is the closest in alignment with the parental construct (Fig. 2A), consistent with the observation that 3-alanine insertion resulted in no functional difference compared to the no-alanine parental construct.

CAR scFv sequence hybridization yields superior CD20 CAR variant

Despite the improvements seen with alanine insertion, the rituximab CAR T cells ultimately failed to effectively control tumor growth *in vivo*. We thus set out to explore additional CAR protein design parameters that could further enhance CAR T–cell function. Two prior studies discussed strategies to alter CAR T–cell function by making changes to the framework region (FR) of the scFv. In the first study, the FR and complementarity-determining regions (CDRs) of the FMC63 CD19 scFv and 14g2a GD2 scFv were intermixed to form hybrid CARs, but no improved CAR variant resulted from this approach, in part due to failure in CAR protein expression that may have resulted from protein misfolding (50). In the second case, CARs targeting chondroitin sulfate proteoglycan 4 (CSPG4) were generated using scFv sequences taken from early- versus late-passages of the 763.74 hybridoma, thus the method relied on the chance occurrence of sequence mutations in hybridoma clones (51). In both studies, CAR protein aggregation at the cell surface was cited as the cause of CAR T–cell dysfunction (50,51). However, as previously noted, rituximab-based CD20 CAR T cells exhibited suboptimal function even though the CAR did not show the formation of macroclusters observed in these earlier studies (Fig. 1E,F), indicating a fundamentally different mechanism at play.

As an alternative approach, we applied a concept similar to DNA shuffling in protein evolution (52), and recombined sequences from two different anti-CD20 scFvs. This hybridization approach allowed exploration of novel CAR sequence space while maximizing the probability of success, as the parent sequences are already "solutions" (i.e., functional in CD20 binding). An scFv molecule comprises a light chain and a heavy chain, and each chain can be further subdivided into three CDRs interspersed among four FRs (Fig. 3A). CDRs closely interact with the target antigen while FRs primarily provide structural support for the variable chains; this division of labor underpins the practice of humanizing antibodies by grafting murine CDRs onto human FRs (53). Given this baseline level of modularity in scFv architecture, we reasoned that it should be possible to recombine the CDRs and FRs of related scFv sequences to generate novel scFv domains that fold properly and retain ligand-binding specificity.

As a partner for rituximab, we chose Leu16, a CD20-specific antibody that has been incorporated into CAR constructs evaluated in the clinic (18,19,54) for three main reasons. First, Leu16-based CARs have been studied in both preclinical and clinical settings. Clinical reports suggest that Leu16-based CAR T cells are safe and—in the context of CD19/CD20 bispecific CARs—could be highly efficacious (18,19,54–57), thus the Leu16 CAR serves as a clinically relevant comparison for the rituximab CAR. Second, since scFv hybridization involves the grafting of CDRs from one scFv onto the frameworks of another scFv, the resulting hybrid protein could misfold or otherwise fail to express. To reduce the possibility of generating dysfunctional variants, we searched for a closely related sequence to serve as hybridization partner for rituximab. Alignment results from T-Coffee (58) showed that V_L and V_H sequences from rituximab and Leu16 are 91% and 92% identical, respectively (Supplementary Fig. S3A), making Leu16 a promising candidate for hybridization with rituximab. Third, rituximab and Leu16 share the same CDR classes (Supplementary Fig. S3B) (59) and overlapping binding epitopes on CD20 (60), two properties that could help minimize the possibility of altered antigen recognition upon scFv sequence hybridization.

We constructed hybrid CARs whose scFv comprised the FRs of rituximab and CDRs of Leu16 (RFR–LCDR), or vice versa (LFR–RCDR) (Fig. 3A). The RFR–LCDR and LFR–RCDR hybrids differ from the rituximab CAR in 11 and 9 amino acid residues, respectively. Both hybrid CARs expressed well on the cell surface, at levels comparable to those of the parental Leu16 and rituximab CARs (Supplementary Fig. S3C,D). All CARs tested, including the CD19 CAR, existed in both monomeric and dimeric forms (Supplementary Fig. S3E); this is expected because the extracellular spacer in all of the tested CARs contains IgG4 hinge, which is capable of forming homodimers via a disulfide bond. However, CAR dimerization did not lead to macro-scale CAR clustering—Leu16 and hybrid CD20 CARs showed even distribution across the cell membrane (Supplementary Fig. S3F), similar to the rituximab CAR and CD19 CAR (Fig. 1F). Notably, RFR–LCDR hybrid CAR T cells exhibited robust tumor-cell lysis and T-cell proliferation upon repeated antigen challenge *in vitro* with Raji lymphoma cells, demonstrating comparable efficacy as the CD19 CAR and superiority over the Leu16-based CD20 CAR (Fig. 3B). In contrast, the LFR–RCDR hybrid—despite being expressed on the cell surface—did not respond to CD20 stimulation (Fig. 3B), and was excluded from further characterization. Henceforth, the term "hybrid CAR" refers to the RFR–LCDR variant. The T-cell subtype distribution based on CD45RA

and CD62L expression was clearly different between CAR-expressing T cells and T cells expressing only the transduction marker EGFRt, but there was no dramatic difference among T cells expressing the CD19 CAR or the various CD20 CARs (Supplementary Fig. S4A).

To understand whether the improved activity of the hybrid CAR may have resulted from a change in ligand-binding affinity, bio-layer interferometry analysis was performed on both parental scFvs (rituximab and Leu16) as well as the RFR–LCDR hybrid scFv. Results showed the CD20 epitope had a slightly stronger binding affinity for the hybrid scFv compared to either of the parent sequences (Supplementary Fig. S4B,C). To further understand whether changes in scFv binding affinity may have affected the antigen sensitivity of CD20 CARs, we evaluated the antigen-detection threshold of different CD20 CAR constructs by co-incubating CD20 CAR T cells with K562 cell lines that express CD20 at varying levels (Supplementary Fig. S4D). Variations in CAR construct had no observable effect on antigen-detection thresholds when the CAR T cells were challenged with target cells expressing varying levels of CD20 antigen. We also did not observe off-target killing by T cells expressing the modified CD20 CAR constructs against the parental $CD20^{-}$ cell line (Supplementary Fig. S4D). Therefore, changes in antigen-detection capability are unlikely to be a key driver for the improved *in vitro* tumor lysis observed with hybrid CAR T cells.

We next performed head-to-head *in vivo* comparisons of the hybrid CAR against each of its parent constructs as well as the CD19 CAR (Fig. 3C–3F). In contrast to both Leu16 and rituximab-based CAR-T cells, RFR–LCDR CAR-T cells efficiently rejected both the original tumor and a tumor re-challenge applied 55 days after initial T-cell treatment (Fig. 3D,E), outperforming the CD19 CAR in eradicating B-cell lymphoma xenografts.

Consistent with previous results, insertion of 2 alanines improved tumor control by rituximab CAR T cells. We further explored whether combining scFv hybridization and alanine insertion would result in added improvements in CAR T cell function. The resulting RFR–LCDR.AA CAR expressed on the cell surface (Supplementary Fig. S4E), conferred perfect protection against both primary tumor and re-challenge (Fig. 3D,E), and drove superior *in vivo* T-cell persistence compared to all other CD20 CAR constructs tested (Fig. 3F).

In the *in vivo* assays presented thus far, tumor-bearing mice were treated with two low doses of CAR T cells. Although split-dose regimens have been evaluated in the clinic (61), the more common treatment modality for lymphoma involves administering a single dose of CAR T cells. Therefore, we performed an *in vivo* study in which animals were treated with a single dose of CAR T cells and re-challenged twice with tumor cells, with escalating tumor dosage levels. The results confirmed robust efficacy of the hybrid CAR T cells (Supplementary Fig. S5). Taken together, these results indicate that the functionality of a CAR can be significantly improved by small changes to the scFv sequence, without altering the target antigen or antigen-detection threshold. Further, we were able to demonstrate the superiority of an RFR–LCDR.AA CD20 CAR in our *in vitro* and *in vivo* assays over two clinically relevant benchmarks—the FMC63 scFv-based CD19 CAR and the Leu16 scFv-based CD20 CAR.

CAR optimization promotes memory formation and strong T-cell effector function

To understand why the hybrid CAR outperformed both parental constructs, we performed RNA-seq on CD20 CAR T cells before and after exposure to established Raji xenografts *in vivo*. Rituximab, Leu16, RFR–LCDR, and RFR–LCDR.AA CAR T cells were recovered from tumor-bearing animals 9 days after receiving a single dose of CAR T cells (Supplementary Fig. S6). Mice treated with the negative-control EGFRt-only T cells did not yield sufficient T cells to enable proper data analysis, consistent with lack of T-cell expansion in the absence of CAR signaling.

Antigen-stimulated RFR–LCDR.AA CAR T cells exhibited a transcriptional signature that was farthest removed from that of rituximab CAR T cells (Fig. 4A; Supplementary Data S2). RFR–LCDR and RFR–LCDR.AA CAR T cells showed distinct transcriptional profiles, with RFR–LCDR more closely resembling the Leu16 CAR, indicating alanine insertion had a measurable impact on CAR function even in the hybrid CAR context. In particular, RFR–LCDR.AA CAR T cells showed strong enrichment in gene sets related to IFNγ response, as well as effector functions such as TNFα and IL2 signaling (Clusters II/III, Fig. 4A,B). Compared to all other test groups, RFR–LCDR.AA CAR T cells were most enriched in the memory phenotype with low cell-cycle activity, while exhibiting strong effector function (Fig. 4C; Supplementary Fig. S7).

By comparison, antigen-stimulated rituximab CAR T cells showed significant enrichment in pathways related to both cytokine signaling and negative regulation of T-cell activation (Cluster I, Fig. 4A,B). Rituximab CAR T cells also showed enrichment in natural killer (NK) cell–mediated cytotoxicity, echoing a report that described upregulation of NK-cell signatures in functionally exhausted CAR T cells (62). Rituximab CAR T cells' tendency toward exhaustion was further highlighted by increased expression of the inhibitory receptors KIR2DL1, KIR2DL3, and KIR3DL1(63), which was observable at both transcriptomic and epigenetic levels (Fig. 4D,E; Supplementary Data S2, S3).

To evaluate whether differences in CAR T–cell biology prior to antigen stimulation contributed to the divergence of transcriptomic profiles after antigen stimulation, we also examined the CAR T cells' transcriptomic profile prior to antigen exposure. Unstimulated rituximab CAR T cells showed elevated expression of *TBX21*, *PRDM1*, and *IRF7*, three effector-function markers previously shown to negatively correlate with clinical response when expressed in T cells prior to antigen exposure (64) (Fig. 4F; Supplementary Data S2, S4). After antigen stimulation, rituximab CAR T cells exhibited the highest *TOX* expression and the lowest *TCF7* and *LEF1* expression among all CAR T–cell variants tested (Fig. 4F), suggesting the emergence of exhausted T cells (65–67). In contrast, unstimulated Leu16, RFR–LCDR, and RFR–LCDR.AA CAR T cells each displayed moderate levels of *TBX21*, *PRDM1*, and *IRF7* (Fig. 4F). Upon antigen stimulation, RFR–LCDR.AA CAR T cells most strongly upregulated effector signatures (*TBX21*, *PRDM1*, and *IRF7*) as well as *TCF7* and *LEF1* expression, but greatly reduced *TOX* expression (Fig. 4F), exhibiting a pattern consistent with progenitor cells transitioning to memory phenotype upon antigen stimulation (65,66). Taken together, these results suggest RFR–LCDR.AA CAR T cells achieved superior *in vivo* antitumor efficacy by responding to antigen stimulation in a more

productive manner, combining strong effector function with the memory phenotype that is conducive to long-term persistence.

DISCUSSION

In this study, we used rational protein design to expand the CD20 CAR protein sequence search space to identify CAR variants that can improve *in vivo* function. We developed a CD20 CAR, termed RFR–LCDR.AA, that incorporated scFv sequence hybridization and alanine insertion to enable robust *in vivo* antitumor efficacy while maintaining relatively low cell-cycle activity levels upon antigen stimulation. In our experience, RFR–LCDR.AA is the first example of a CD20 CAR that can outperform the FMC63-based CD19 CAR in head-to-head comparisons using the Raji B-cell lymphoma xenograft model. Coupled with strong activation and effector functions, RFR LCDR.AA CAR-T cells' memory-like phenotype is reminiscent of prior reports of "metabolically plastic" T cells that efficiently adapt to changing environments upon tumor encounters, resulting in increased antitumor efficacy (68). Moreover, enrichment of memory in CD19 CAR T–cell patient products has been shown to correlate with durable complete responses (69,70), bolstering the likelihood of durable efficacy by RFR–LCDR.AA CAR T cells upon clinical translation. Of note, the RFR–LCDR.AA CAR is 98% identical to both the rituximab CAR (differing in 13 out of 661 residues) and the Leu16 CAR (differing in 11 out of 661 residues), illustrating the criticality of the *precise* CAR protein sequence to CAR T–cell function.

As a protein-engineering strategy, alanine insertion is readily adaptable to any CAR of interest. However, the functional improvements resulting from alanine insertion were modest albeit statistically significant. A second, complementary protein-engineering strategy, scFv hybridization, resulted in substantially greater improvements in CAR T–cell function. By recombining the FRs and CDRs of rituximab and Leu16 scFvs, we generated two hybrid CARs that both expressed well, but only one could recognize the CD20 antigen, underscoring the need for empirical validation in addition to rational protein design. Unlike alanine insertion, scFv hybridization is a sequence-dependent strategy, and the availability of parent sequences with sufficient similarity increases the likelihood of generating hybrids capable of proper protein folding. The fact that multiple mAbs are often available for a given clinically relevant target antigen offers a starting point for this engineering strategy. Moving forward, in-depth analysis of protein structure and site-specific mutations may allow for precise identification of truly critical residues, and enable a fully rational approach to scFv design. Moreover, altering the scFv sequence could impact the antigen specificity and thus the safety of the clinical product. Assessments on antigen specificity and unexpected off-target effects would be critical in the evaluation of clinical candidates that result from this engineering approach.

Collectively, we demonstrated that judicial design of CAR protein sequences is critical to CAR T–cell function, and even minute changes in amino-acid sequences can lead to significant alterations in CAR T–cell function, accompanied by marked shifts in transcriptional and epigenetic profiles upon antigen stimulation. Highly functional CD20 CAR T cells transition to a memory phenotype that is high in effector function but low in cell-cycle activity upon antigen stimulation. In this work, we examined the effects of

changing protein conformation and scFv sequence on CAR T–cell function. The findings of this study could be complementary to the CAR design principles elucidated by prior studies, including the importance of ligand-binding affinity, extracellular spacer length and rigidity, choice of co-stimulatory signals, and potential for tonic signaling. Moreover, the RFR–LCDR.AA CAR is a promising candidate for clinical translation, and findings from this study could serve as a useful reference in characterizing future CAR designs aimed at providing functionally robust CAR T–cell therapy for advanced malignancies.

Supplementary Material

Refer to Web version on PubMed Central for supplementary material.

ACKNOWLEDGMENTS

We thank Drs. Anna M. Wu and Kirstin A. Zettlitz for helpful discussions on anti-CD20 scFv sequences. We thank Dr. Willy Hugo and Katherine M. Sheu for helpful guidance and discussions on RNA-seq data analysis. We thank Wallace Wennerberg, Jaimie Chen, Sabah Rahman, Brenda Ji, Paul Ayoub, Duo Xu, and Zheng Cao for their technical assistance. We thank Suhua Feng, Marco Morselli, Shawn Cokus and Mahnaz Akhavan (UCLA BSCRC BioSequencing Core Facility) and the UCLA Molecular Instrument Center for their technical support. This work was supported by funding from the Alliance for Cancer Gene Therapy (Young Investigator Award to YYC) and the Cancer Research Institute (Lloyd J. Old STAR Award to YYC). This work was performed with instrumentation and computational resources from the Eli and Edythe Broad Center of Regenerative Medicine and Stem Cell Research – Molecular, Cell, and Developmental Biology Microscopy Core, the UCLA Jonsson Comprehensive Cancer Center (JCCC) Flow Cytometry Core Facility supported by the National Institutes of Health (P30 CA016042), and the Hoffman2 Shared Cluster provided by the UCLA Institute for Digital Research and Education's Research Technology Group.

Funding information:

- Alliance for Cancer Gene Therapy grant 20161602 (YYC)
- Cancer Research Institute Lloyd J. Old STAR Award (YYC)

Authors Disclosures:

YYC and XC are inventors of patents whose value may be affected by the publication of this study. XC is an employee of and stock-option holder of ImmPACT Bio. ES is an employee of Instil Bio. YYC is a founder of, holds equity in, and receives consulting fees from ImmPACT Bio. YYC is a member of the scientific advisory board of and holds stock options in Catamaran Bio, Notch Therapeutics, Pluto Immunotherapeutics, Prime Medicine, Sonoma Biotherapeutics, and Waypoint Bio. The other authors declare no competing interest.

REFERENCES

1. Frigault MJ, Maus MV. State of the art in CAR T cell therapy for CD19+ B cell malignancies. J Clin Invest 2020;130(4):1586–94 doi 10.1172/JCI129208. [PubMed: 32235098]
2. Majzner RG, Mackall CL. Clinical lessons learned from the first leg of the CAR T cell journey. Nat Med 2019;25(9):1341–55 doi 10.1038/s41591-019-0564-6. [PubMed: 31501612]
3. Shih RM, Chen YY. Engineering Principles for Synthetic Biology Circuits in Cancer Immunotherapy. Cancer Immunol Res 2022;10(1):6–11 doi 10.1158/2326-6066.CIR-21-0769. [PubMed: 34983828]
4. Ruella M, Maus MV. Catch me if you can: Leukemia Escape after CD19-Directed T Cell Immunotherapies. Comput Struct Biotechnol J 2016;14:357–62 doi 10.1016/j.csbj.2016.09.003. [PubMed: 27761200]
5. Hsieh EM, Rouce RH. Chimeric antigen receptor T cells for mature B-cell lymphoma and Burkitt lymphoma. Hematology Am Soc Hematol Educ Program 2020;2020(1):487–93 doi 10.1182/hematology.2020000133. [PubMed: 33275669]

6. Gardner RA, Finney O, Annesley C, Brakke H, Summers C, Leger K, et al. Intent-to-treat leukemia remission by CD19 CAR T cells of defined formulation and dose in children and young adults. Blood 2017;129(25):3322–31 doi 10.1182/blood-2017-02-769208. [PubMed: 28408462]
7. Lee DW, Kochenderfer JN, Stetler-Stevenson M, Cui YK, Delbrook C, Feldman SA, et al. T cells expressing CD19 chimeric antigen receptors for acute lymphoblastic leukaemia in children and young adults: a phase 1 dose-escalation trial. Lancet 2015;385(9967):517–28 doi 10.1016/s0140-6736(14)61403-3. [PubMed: 25319501]
8. Maude SL, Frey N, Shaw PA, Aplenc R, Barrett DM, Bunin NJ, et al. Chimeric Antigen Receptor T Cells for Sustained Remissions in Leukemia. New England Journal of Medicine 2014;371(16):1507–17 doi 10.1056/NEJMoa1407222. [PubMed: 25317870]
9. Maude SL, Laetsch TW, Buechner J, Rives S, Boyer M, Bittencourt H, et al. Tisagenlecleucel in Children and Young Adults with B-Cell Lymphoblastic Leukemia. N Engl J Med 2018;378(5):439–48 doi 10.1056/NEJMoa1709866. [PubMed: 29385370]
10. Neelapu SS, Rossi JM, Jacobson CA, Locke FL, Miklos DB, Reagan PM, et al. CD19-Loss with Preservation of Other B Cell Lineage Features in Patients with Large B Cell Lymphoma Who Relapsed Post-Axi-Cel. Blood 2019;134(Supplement_1):203- doi 10.1182/blood-2019-126218.
11. Schneider D, Xiong Y, Wu D, Hu P, Alabanza L, Steimle B, et al. Trispecific CD19-CD20-CD22-targeting duoCAR-T cells eliminate antigen-heterogeneous B cell tumors in preclinical models. Sci Transl Med 2021;13(586) doi 10.1126/scitranslmed.abc6401.
12. Schneider D, Xiong Y, Wu D, Nlle V, Schmitz S, Haso W, et al. A tandem CD19/CD20 CAR lentiviral vector drives on-target and off-target antigen modulation in leukemia cell lines. J Immunother Cancer 2017;5:42 doi 10.1186/s40425-017-0246-1. [PubMed: 28515942]
13. Zah E, Lin MY, Silva-Benedict A, Jensen MC, Chen YY. T Cells Expressing CD19/CD20 Bispecific Chimeric Antigen Receptors Prevent Antigen Escape by Malignant B Cells. Cancer Immunol Res 2016;4(6):498–508 doi 10.1158/2326-6066.CIR-15-0231. [PubMed: 27059623]
14. Bos TJ, De Bruyne E, Van Lint S, Heirman C, Vanderkerken K. Large double copy vectors are functional but show a size-dependent decline in transduction efficiency. J Biotechnol 2010;150(1):37–40 doi 10.1016/j.jbiotec.2010.07.010. [PubMed: 20638430]
15. Kumar M, Keller B, Makalou N, Sutton RE. Systematic determination of the packaging limit of lentiviral vectors. Hum Gene Ther 2001;12(15):1893–905 doi 10.1089/104303401753153947. [PubMed: 11589831]
16. Shalabi H, Kraft IL, Wang HW, Yuan CM, Yates B, Delbrook C, et al. Sequential loss of tumor surface antigens following chimeric antigen receptor T-cell therapies in diffuse large B-cell lymphoma. Haematologica 2018;103(5):e215–e8 doi 10.3324/haematol.2017.183459. [PubMed: 29419431]
17. Johnson NA, Leach S, Woolcock B, deLeeuw RJ, Bashashati A, Sehn LH, et al. CD20 mutations involving the rituximab epitope are rare in diffuse large B-cell lymphomas and are not a significant cause of R-CHOP failure. Haematologica 2009;94(3):423–7 doi 10.3324/haematol.2008.001024. [PubMed: 19211644]
18. Till BG, Jensen MC, Wang J, Chen EY, Wood BL, Greisman HA, et al. Adoptive immunotherapy for indolent non-Hodgkin lymphoma and mantle cell lymphoma using genetically modified autologous CD20-specific T cells. Blood 2008;112(6):2261–71 doi 10.1182/blood-2007-12-128843. [PubMed: 18509084]
19. Till BG, Jensen MC, Wang J, Qian X, Gopal AK, Maloney DG, et al. CD20-specific adoptive immunotherapy for lymphoma using a chimeric antigen receptor with both CD28 and 4-1BB domains: pilot clinical trial results. Blood 2012;119(17):3940–50 doi 10.1182/blood-2011-10-387969. [PubMed: 22308288]
20. Wang Y, Zhang WY, Han QW, Liu Y, Dai HR, Guo YL, et al. Effective response and delayed toxicities of refractory advanced diffuse large B-cell lymphoma treated by CD20-directed chimeric antigen receptor-modified T cells. Clin Immunol 2014;155(2):160–75 doi 10.1016/j.clim.2014.10.002. [PubMed: 25444722]
21. Zhang WY, Wang Y, Guo YL, Dai HR, Yang QM, Zhang YJ, et al. Treatment of CD20-directed Chimeric Antigen Receptor-modified T cells in patients with relapsed or refractory B-cell non-Hodgkin lymphoma: an early phase IIa trial report. Signal Transduct Target Ther 2016;1:16002 doi 10.1038/sigtrans.2016.2. [PubMed: 29263894]

22. Liang A, Ye S, Li P, Huang J, Zhu S, Yao X, et al. Safety and efficacy of a novel anti-CD20 chimeric antigen receptor (CAR)-T cell therapy in relapsed/refractory (r/r) B-cell non-Hodgkin lymphoma (B-NHL) patients after failing CD19 CAR-T therapy. Journal of Clinical Oncology 2021;39(15_suppl):2508- doi 10.1200/JCO.2021.39.15_suppl.2508.

23. Shadman M, Yeung C, Redman MW, Lee SY, Lee DH, Ramachandran A, et al. Third Generation CD20 Targeted CAR T-Cell Therapy (MB-106) for Treatment of Patients with Relapsed/Refractory B-Cell Non-Hodgkin Lymphoma. Blood 2020;136(Supplement 1):38–9 doi 10.1182/blood-2020-136440.

24. Shadman M, Yeung CCS, Redman MW, Lee SY, Lee DH, Ra S, et al. Safety and Efficacy of Third Generation CD20 Targeted CAR-T (MB-106) for Treatment of Relapsed/Refractory B-NHL and CLL. Journal of Clinical Oncology 2021;39(15).

25. Zettlitz KA, Tavare R, Knowles SM, Steward KK, Timmerman JM, Wu AM. ImmunoPET of Malignant and Normal B Cells with (89)Zr- and (124)I-Labeled Obinutuzumab Antibody Fragments Reveals Differential CD20 Internalization In Vivo. Clin Cancer Res 2017;23(23):7242–52 doi 10.1158/1078-0432.CCR-17-0855. [PubMed: 28928164]

26. Nicholson IC, Lenton KA, Little DJ, Decorso T, Lee FT, Scott AM, et al. Construction and characterisation of a functional CD19 specific single chain Fv fragment for immunotherapy of B lineage leukaemia and lymphoma. Mol Immunol 1997;34(16-17):1157–65. [PubMed: 9566763]

27. Hawley RG, Lieu FH, Fong AZ, Hawley TS. Versatile retroviral vectors for potential use in gene therapy. Gene Ther 1994;1(2):136–8. [PubMed: 7584069]

28. Hughes MS, Yu YY, Dudley ME, Zheng Z, Robbins PF, Li Y, et al. Transfer of a TCR gene derived from a patient with a marked antitumor response conveys highly active T-cell effector functions. Hum Gene Ther 2005;16(4):457–72 doi 10.1089/hum.2005.16.457. [PubMed: 15871677]

29. Ho P, Ede C, Chen YY. Modularly Constructed Synthetic Granzyme B Molecule Enables Interrogation of Intracellular Proteases for Targeted Cytotoxicity. ACS Synth Biol 2017;6(8):1484–95 doi 10.1021/acssynbio.6b00392. [PubMed: 28510446]

30. Jensen M, Tan G, Forman S, Wu AM, Raubitschek A. CD20 is a molecular target for scFvFc:zeta receptor redirected T cells: implications for cellular immunotherapy of CD20+ malignancy. Biol Blood Marrow Transplant 1998;4(2):75–83. [PubMed: 9763110]

31. Los GV, Encell LP, McDougall MG, Hartzell DD, Karassina N, Zimprich C, et al. HaloTag: a novel protein labeling technology for cell imaging and protein analysis. ACS Chem Biol 2008;3(6):373–82 doi 10.1021/cb800025k. [PubMed: 18533659]

32. Zah E, Nam E, Bhuvan V, Tran U, Ji BY, Gosliner SB, et al. Systematically optimized BCMA/CS1 bispecific CAR-T cells robustly control heterogeneous multiple myeloma. Nat Commun 2020;11(1):2283 doi 10.1038/s41467-020-16160-5. [PubMed: 32385241]

33. Buenrostro JD, Giresi PG, Zaba LC, Chang HY, Greenleaf WJ. Transposition of native chromatin for fast and sensitive epigenomic profiling of open chromatin, DNA-binding proteins and nucleosome position. Nat Methods 2013;10(12):1213–8 doi 10.1038/nmeth.2688. [PubMed: 24097267]

34. Corces MR, Trevino AE, Hamilton EG, Greenside PG, Sinnott-Armstrong NA, Vesuna S, et al. An improved ATAC-seq protocol reduces background and enables interrogation of frozen tissues. Nat Methods 2017;14(10):959–62 doi 10.1038/nmeth.4396. [PubMed: 28846090]

35. Spinelli L, Carpentier S, Montanana Sanchis F, Dalod M, Vu Manh TP. BubbleGUM: automatic extraction of phenotype molecular signatures and comprehensive visualization of multiple Gene Set Enrichment Analyses. BMC Genomics 2015;16:814 doi 10.1186/s12864-015-2012-4. [PubMed: 26481321]

36. Kuleshov MV, Jones MR, Rouillard AD, Fernandez NF, Duan Q, Wang Z, et al. Enrichr: a comprehensive gene set enrichment analysis web server 2016 update. Nucleic Acids Res 2016;44(W1):W90–7 doi 10.1093/nar/gkw377. [PubMed: 27141961]

37. Salles G, Barrett M, Foa R, Maurer J, O'Brien S, Valente N, et al. Rituximab in B-Cell Hematologic Malignancies: A Review of 20 Years of Clinical Experience. Adv Ther 2017;34(10):2232–73 doi 10.1007/s12325-017-0612-x. [PubMed: 28983798]

38. Hudecek M, Sommermeyer D, Kosasih PL, Silva-Benedict A, Liu L, Rader C, et al. The nonsignaling extracellular spacer domain of chimeric antigen receptors is decisive for in vivo

antitumor activity. Cancer Immunol Res 2015;3(2):125–35 doi 10.1158/2326-6066.CIR-14-0127. [PubMed: 25212991]

39. Jonnalagadda M, Mardiros A, Urak R, Wang X, Hoffman LJ, Bernanke A, et al. Chimeric antigen receptors with mutated IgG4 Fc spacer avoid fc receptor binding and improve T cell persistence and antitumor efficacy. Mol Ther 2015;23(4):757–68 doi 10.1038/mt.2014.208. [PubMed: 25366031]
40. Frigault MJ, Lee J, Basil MC, Carpenito C, Motohashi S, Scholler J, et al. Identification of chimeric antigen receptors that mediate constitutive or inducible proliferation of T cells. Cancer Immunol Res 2015;3(4):356–67 doi 10.1158/2326-6066.CIR-14-0186. [PubMed: 25600436]
41. Singh N, Frey NV, Engels B, Barrett DM, Shestova O, Ravikumar P, et al. Antigen-independent activation enhances the efficacy of 4-1BB-costimulated CD22 CAR T cells. Nat Med 2021;27(5):842–50 doi 10.1038/s41591-021-01326-5. [PubMed: 33888899]
42. Wang X, Phan MM, Sun Y, Koerber JT, Ho H, Chen Y, et al. Development of an SPR-based binding assay for characterization of anti-CD20 antibodies to CD20 expressed on extracellular vesicles. Anal Biochem 2022;646:114635 doi 10.1016/j.ab.2022.114635. [PubMed: 35278435]
43. Hartman NC, Groves JT. Signaling clusters in the cell membrane. Curr Opin Cell Biol 2011;23(4):370–6 doi 10.1016/j.ceb.2011.05.003. [PubMed: 21665455]
44. Wu H, Cao R, Wen M, Xue H, OuYang B. Structural characterization of a dimerization interface in the CD28 transmembrane domain. Structure 2022;30(6):803–12 e5 doi 10.1016/j.str.2022.03.004. [PubMed: 35397202]
45. Constantinescu SN, Keren T, Socolovsky M, Nam H, Henis YI, Lodish HF. Ligand-independent oligomerization of cell-surface erythropoietin receptor is mediated by the transmembrane domain. Proc Natl Acad Sci U S A 2001;98(8):4379–84 doi 10.1073/pnas.081069198. [PubMed: 11296286]
46. Liu W, Kawahara M, Ueda H, Nagamune T. Construction of a fluorescein-responsive chimeric receptor with strict ligand dependency. Biotechnol Bioeng 2008;101(5):975–84 doi 10.1002/bit.21961. [PubMed: 18500765]
47. Scheller L, Strittmatter T, Fuchs D, Bojar D, Fussenegger M. Generalized extracellular molecule sensor platform for programming cellular behavior. Nat Chem Biol 2018;14(7):723–9 doi 10.1038/s41589-018-0046-z. [PubMed: 29686358]
48. Arai R, Wriggers W, Nishikawa Y, Nagamune T, Fujisawa T. Conformations of variably linked chimeric proteins evaluated by synchrotron X-ray small-angle scattering. Proteins 2004;57(4):829–38 doi 10.1002/prot.20244. [PubMed: 15390267]
49. Carpenito C, Milone MC, Hassan R, Simonet JC, Lakhal M, Suhoski MM, et al. Control of large, established tumor xenografts with genetically retargeted human T cells containing CD28 and CD137 domains. Proc Natl Acad Sci U S A 2009;106(9):3360–5 doi 10.1073/pnas.0813101106. [PubMed: 19211796]
50. Long AH, Haso WM, Shern JF, Wanhainen KM, Murgai M, Ingaramo M, et al. 4-1BB costimulation ameliorates T cell exhaustion induced by tonic signaling of chimeric antigen receptors. Nat Med 2015;21(6):581–90 doi 10.1038/nm.3838. [PubMed: 25939063]
51. Landoni E, Fuca G, Wang J, Chirasani VR, Yao Z, Dukhovlinova E, et al. Modifications to the Framework Regions Eliminate Chimeric Antigen Receptor Tonic Signaling. Cancer Immunol Res 2021;9(4):441–53 doi 10.1158/2326-6066.CIR-20-0451. [PubMed: 33547226]
52. Simon AJ, d'Oelsnitz S, Ellington AD. Synthetic evolution. Nat Biotechnol 2019;37(7):730–43 doi 10.1038/s41587-019-0157-4. [PubMed: 31209374]
53. Safdari Y, Farajnia S, Asgharzadeh M, Khalili M. Antibody humanization methods - a review and update. Biotechnol Genet Eng Rev 2013;29:175–86 doi 10.1080/02648725.2013.801235. [PubMed: 24568279]
54. Shah NN, Johnson BD, Schneider D, Zhu F, Szabo A, Keever-Taylor CA, et al. Bispecific anti-CD20, anti-CD19 CAR T cells for relapsed B cell malignancies: a phase 1 dose escalation and expansion trial. Nat Med 2020;26(10):1569–75 doi 10.1038/s41591-020-1081-3. [PubMed: 33020647]

55. Zhang Y, Wang Y, Liu Y, Tong C, Wang C, Guo Y, et al. Long-term activity of tandem CD19/CD20 CAR therapy in refractory/relapsed B-cell lymphoma: a single-arm, phase 1-2 trial. Leukemia 2022;36(1):189–96 doi 10.1038/s41375-021-01345-8. [PubMed: 34272481]
56. Tong C, Zhang Y, Liu Y, Ji X, Zhang W, Guo Y, et al. Optimized tandem CD19/CD20 CAR-engineered T cells in refractory/relapsed B-cell lymphoma. Blood 2020;136(14):1632–44 doi 10.1182/blood.2020005278. [PubMed: 32556247]
57. Larson SM, Walthers C, Ji B, Ghafouri SN, Naparstek J, Trent J, et al. CD19/CD20 bispecific chimeric antigen receptor (CAR) in naïve/memory T cells for the treatment of relapsed or refractory non-Hodgkin lymphoma. Journal of Clinical Oncology 2022;40(16_suppl):2543- doi 10.1200/JCO.2022.40.16_suppl.2543.
58. Notredame C, Higgins DG, Heringa J. T-Coffee: A novel method for fast and accurate multiple sequence alignment. J Mol Biol 2000;302(1):205–17 doi 10.1006/jmbi.2000.4042. [PubMed: 10964570]
59. Swindells MB, Porter CT, Couch M, Hurst J, Abhinandan KR, Nielsen JH, et al. abYsis: Integrated Antibody Sequence and Structure-Management, Analysis, and Prediction. J Mol Biol 2017;429(3):356–64 doi 10.1016/j.jmb.2016.08.019. [PubMed: 27561707]
60. Rufener GA, Press OW, Olsen P, Lee SY, Jensen MC, Gopal AK, et al. Preserved Activity of CD20-Specific Chimeric Antigen Receptor-Expressing T Cells in the Presence of Rituximab. Cancer Immunol Res 2016;4(6):509–19 doi 10.1158/2326-6066.CIR-15-0276. [PubMed: 27197068]
61. Rouce RH, Fousek K, Ahmed N, Gottschalk S, Savoldo B, Dotti G, et al. Safety of Multiple Doses of CAR T Cells. Blood 2015;126(23):4425- doi 10.1182/blood.V126.23.4425.4425.
62. Good CR, Aznar MA, Kuramitsu S, Samareh P, Agarwal S, Donahue G, et al. An NK-like CAR T cell transition in CAR T cell dysfunction. Cell 2021;184(25):6081–100 e26 doi 10.1016/j.cell.2021.11.016. [PubMed: 34861191]
63. Bjorkstrom NK, Beziat V, Cichocki F, Liu LL, Levine J, Larsson S, et al. CD8 T cells express randomly selected KIRs with distinct specificities compared with NK cells. Blood 2012;120(17):3455–65 doi 10.1182/blood-2012-03-416867. [PubMed: 22968455]
64. Chen GM, Chen C, Das RK, Gao P, Chen CH, Bandyopadhyay S, et al. Integrative bulk and single-cell profiling of pre-manufacture T-cell populations reveals factors mediating long-term persistence of CAR T-cell therapy. Cancer Discov 2021;11(9):2186–99 doi 10.1158/2159-8290.CD-20-1677. [PubMed: 33820778]
65. Alfei F, Kanev K, Hofmann M, Wu M, Ghoneim HE, Roelli P, et al. TOX reinforces the phenotype and longevity of exhausted T cells in chronic viral infection. Nature 2019;571(7764):265–9 doi 10.1038/s41586-019-1326-9. [PubMed: 31207605]
66. Khan O, Giles JR, McDonald S, Manne S, Ngiow SF, Patel KP, et al. TOX transcriptionally and epigenetically programs CD8(+) T cell exhaustion. Nature 2019;571(7764):211–8 doi 10.1038/s41586-019-1325-x. [PubMed: 31207603]
67. Scott AC, Dundar F, Zumbo P, Chandran SS, Klebanoff CA, Shakiba M, et al. TOX is a critical regulator of tumour-specific T cell differentiation. Nature 2019;571(7764):270–4 doi 10.1038/s41586-019-1324-y. [PubMed: 31207604]
68. Leone RD, Zhao L, Englert JM, Sun IM, Oh MH, Sun IH, et al. Glutamine blockade induces divergent metabolic programs to overcome tumor immune evasion. Science 2019;366(6468):1013–21 doi 10.1126/science.aav2588. [PubMed: 31699883]
69. Bai Z, Woodhouse S, Zhao Z, Arya R, Govek K, Kim D, et al. Single-cell antigen-specific landscape of CAR T infusion product identifies determinants of CD19-positive relapse in patients with ALL. Sci Adv 2022;8(23):eabj2820 doi 10.1126/sciadv.abj2820. [PubMed: 35675405]
70. Deng Q, Han G, Puebla-Osorio N, Ma MCJ, Strati P, Chasen B, et al. Characteristics of anti-CD19 CAR T cell infusion products associated with efficacy and toxicity in patients with large B cell lymphomas. Nat Med 2020;26(12):1878–87 doi 10.1038/s41591-020-1061-7. [PubMed: 33020644]

SYNOPSIS

Rational protein design yielded a CD20 CAR that outperforms a clinically relevant CD19 CAR in lymphoma models, providing a new candidate for non-Hodgkin lymphoma therapy. This protein-engineering approach could be applied to develop additional CARs against diverse antigens.

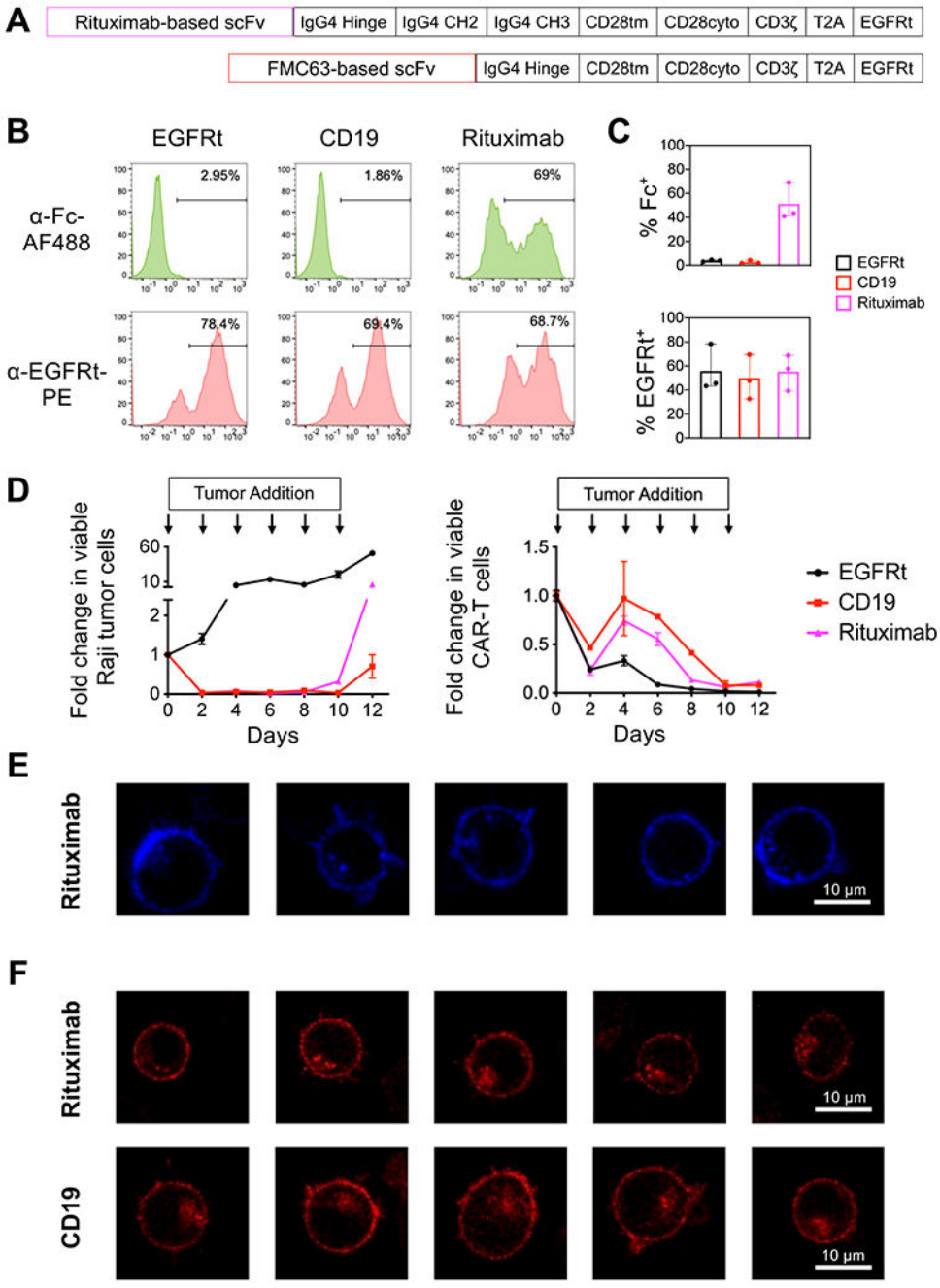

Fig. 1. Rituximab-based CD20 CAR T cells have limited antitumor efficacy and tonically signal.

(**A**) Schematic of rituximab-based CD20 CAR and FMC63-based CD19 CAR. (**B**) CAR surface expression (top) and transduction-marker expression (bottom) detected by flow cytometry via antibody staining of the CAR's IgG4 extracellular spacer (Fc) and EGFRt, respectively. Percent positivity and MFI of each sample are noted. The CD19 CAR does not contain the CH2–CH3 domain of the IgG4 and is thus undetectable by Fc staining. Data are for T cells generated from one healthy donor and representative of the data from three different healthy donors. (**C**) Percent Fc^+ and $EGFRt^+$ for T cells generated from

three different healthy donors. (**D**) CAR T–cell cytotoxicity and proliferation upon repeated antigen challenge *in vitro*. Rituximab-based CD20 CAR T cells, FMC63-based CD19 CAR T cells, or control T cells (transduced to express only the transduction marker, EGFRt) were challenged with $CD19^{+}CD20^{+}$ Raji tumor cells at a 2:1 effector-to-target (E:T) ratio every two days, and the number of viable Raji and CAR T cells was quantified by flow cytometry. Data shown are the means of technical triplicates with error bars indicating ± 1 standard deviation (S.D.). Results are representative of three independent experiments using T cells from three different healthy donors. (**E**) CAR expressing Jurkat cells were stained with an Fc-specific antibody conjugated to DyLight 405 and imaged by confocal microscopy in the absence of antigen stimulation. By this method, only CARs on the cell surface or those that were internalized after having been stained by the Fc-specific antibody on the surface are labeled. (**F**) Jurkat cells transduced with CAR-HaloTag fusion proteins were stained with the red fluorescent dye tetramethylrhodamine (TMR) and imaged by confocal microscopy in the absence of antigen stimulation. TMR Is a cell-permeable dye, thus it stains both intracellular and surface-anchored CAR molecules.

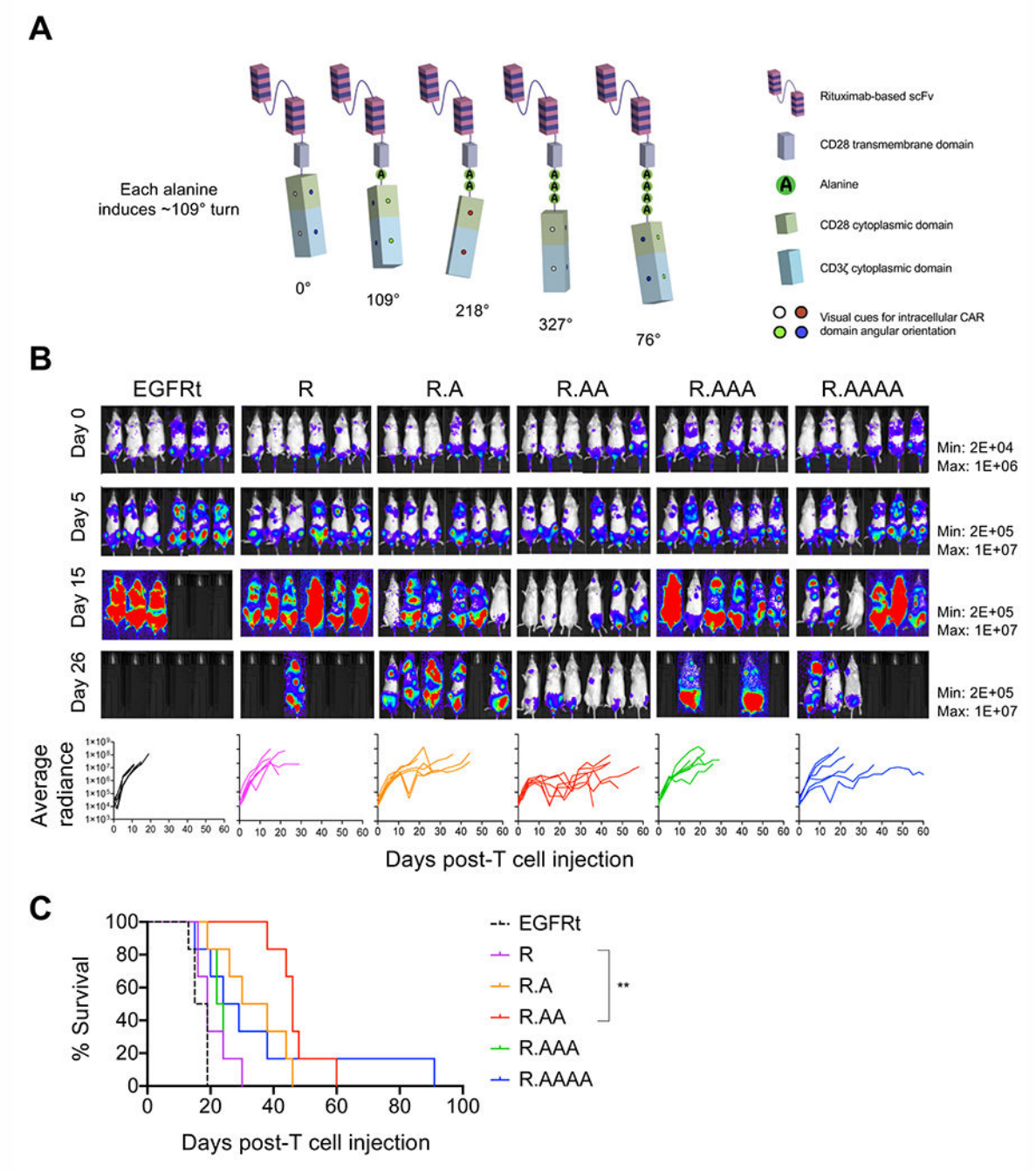

Fig. 2. Torsional reorientation of signaling domain tunes CAR T–cell activity.

(**A**) Schematic of rituximab-based CAR constructs with zero to four alanines inserted between the CD28 transmembrane and cytoplasmic domains. (**B,C**) NSG mice were injected intravenously with 0.5 x 10^6 ffLuc-expressing Raji cells followed by two doses of CAR^+ T cells 6 days (1.35 x 10^6 cells) and 12 days (1.5 x 10^6 cells) later; n = 6 mice per group. (**B**) Tumor progression was monitored by bioluminescence imaging (top). Radiance (in photons/sec/cm^2/sr) of individual animals are shown for each group (bottom). The end point of each trace indicates the humane end point of each animal. (**C**) Kaplan–Meier

survival curve. Statistical significance was determined by log-rank (Mantel-Cox) test with Holm-Sidak correction for multiple comparisons. $^{**}p<0.01$.

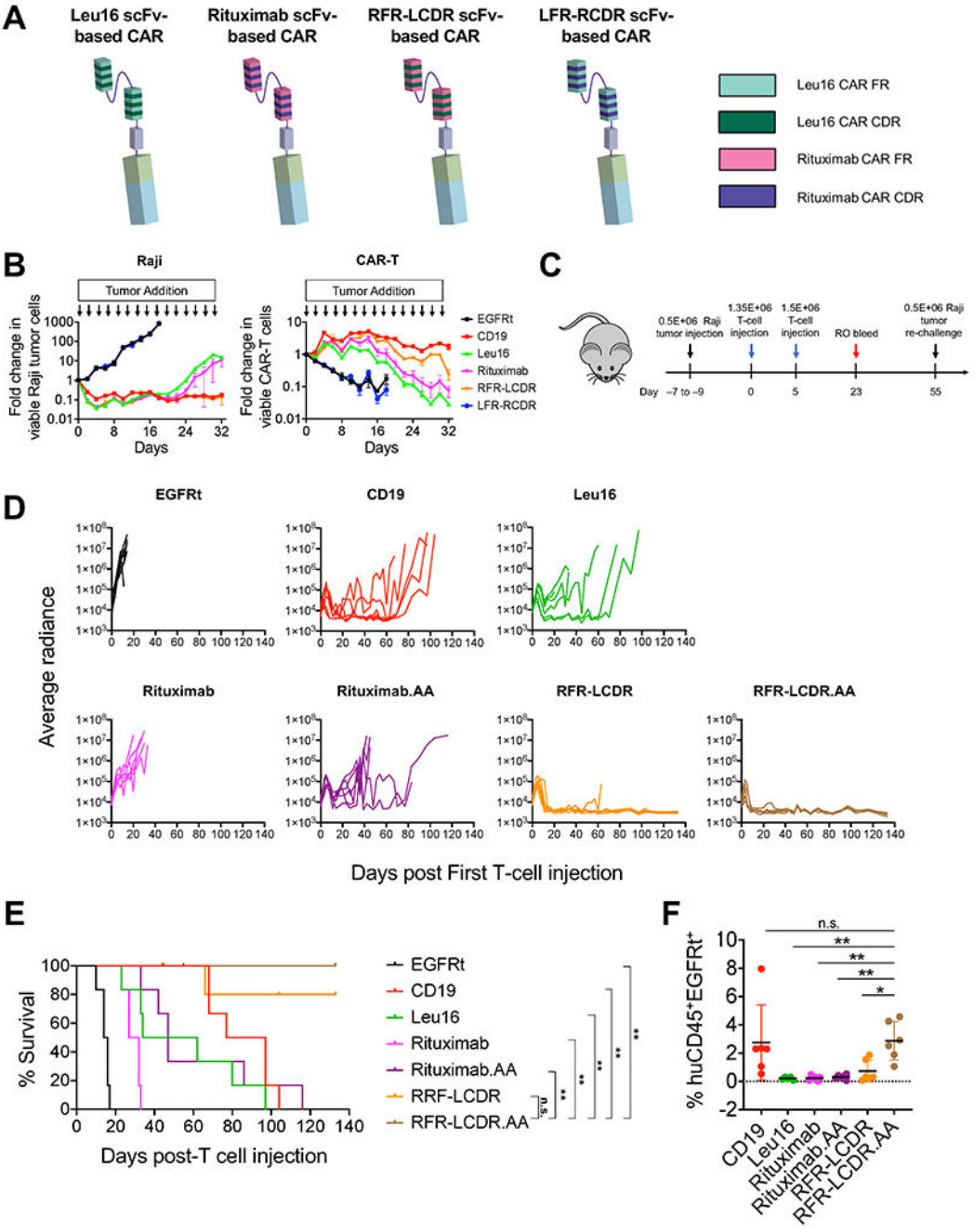

Fig. 3. scFv sequence hybridization in CAR protein further enhances CAR T–cell function *in vivo*.

(**A**) Schematic of scFv sequence hybridization in CAR molecules. The framework regions (FR) and complementarity-determining regions (CDRs) of Leu16- and rituximab-derived scFvs were intermixed to yield two hybrid CAR variants (RFR–LCDR and LFR–RCDR). (**B**) RFR–LCDR hybrid CAR T cells had superior antitumor function and T-cell proliferation compared to parental CAR T cells upon repeated antigen challenge *in vitro*. CAR T cells were challenged with Raji cells at a 2:1 E:T ratio every two days. T-cell and target-cell

counts were quantified by flow cytometry. Data shown are the means of technical triplicates ± 1 S.D. Results are representative of three independent experiments using CAR T cells generated from three different healthy donors. (**C**) Schematic of Raji xenograft model treated with CAR T cells and re-challenged with Raji lymphomas; n = 6 mice per group. (**D**) Tumor signal (in photons/sec/cm^2/sr) in individual animals administered the indicated CAR T cells as quantified by bioluminescence imaging. (**E**) Kaplan–Meier survival curve. Log-rank (Mantel–Cox) test was performed with Holm–Sidak correction for multiple comparisons. Statistical significances of each treatment group compared to treatment with RFR-LCDR.AA are shown. *p<0.05, **p<0.01, ***p<0.001, n.s. not statistically significant. (**F**) Frequency of human $CD45^+EGFRt^+$ cells in peripheral blood collected from mice on day 23 after first dose of T-cell infusion. Data represent mean values with error bars indicating ± 1 S.D. Statistical significance was determined by two-tailed Student's *t* test with Sidak correction for multiple comparisons. Statistical significances of each treatment group compared to treatment with RFR-LCDR.AA are shown. *p<0.05, **p<0.01, ***p<0.001, n.s. not statistically significant.

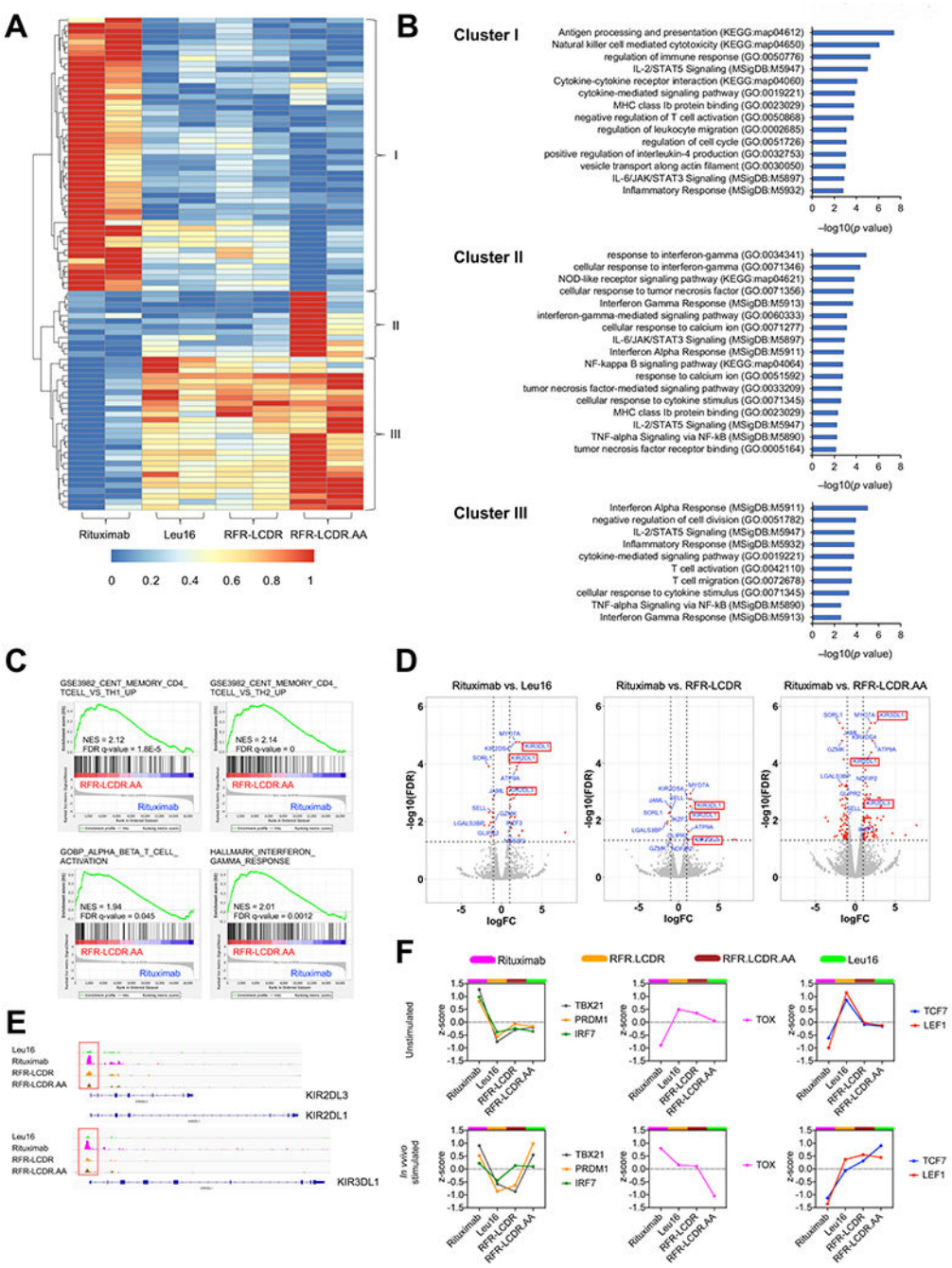

Fig. 4. RFR–LCDR.AA CAR promotes enrichment of memory T cells coupled with strong effector function upon antigen stimulation.

(**A–E**) NSG mice were injected i.v. with 0.5 x 10^6 ffLuc-expressing Raji cells, followed by 2.85 x 10^6 CAR^+ T cells delivered i.v. 6 days later; n = 2 mice per group. Liver, spleen, cardiac blood, and bone marrow were collected from tumor-bearing mice 9 days after T-cell injection as shown in Supplementary Fig. S6. CAR^+ T cells were obtained by sorting for $huCD45^+$ $EGFRt^+$ populations, and subsequently analyzed by RNA-seq and ATAC-seq. (**A**) Heatmap of differentially expressed genes (FDR < 0.05) identified through

ANOVA, with each column representing one mouse. Each row is scaled to a maximum of 1 and minimum of 0 to highlight relative expression of each gene. (**B**) Enriched pathways associated with the different differentially expressed gene clusters, with *p* values shown in −log10 scale. Only pathways with statistically significant adjusted *p* value (<0.05) using the Benjamini–Hochberg method are included. (**C**) Gene set enrichment analysis (GSEA) of RFR–LCDR.AA CAR T cells versus rituximab CAR T cells. (**D**) Volcano plots of differentially expressed genes of rituximab CAR T cells versus Leu16 (left), RFR–LCDR (middle), or RFR–LCDR.AA (right) CAR T cells based on RNA-seq. All differentially expressed genes are plotted in grey. Genes that have at least 2-fold upregulation or downregulation (log2FC > 1 or log2FC < −1) with FDR < 0.05 are shown in red. The names of genes that appear in all three sets of pair-wise comparisons with log2FC > 1 and FDR < 0.05 or log2FC < −1 and FDR < 0.05 are labeled. (**E**) Genome browser files of differentially accessible regions based on ATAC-seq in Leu16, rituximab, RFR–LCDR, RFR–LCDR.AA CAR T cells at the *KIR2DL3*, *KIR2DL1*, *KIR3DL1* loci. (**F**) Average z-scores of genes associated with memory/exhausted T-cell progenitors (*TOX*), memory T cells (*TCF7* and *LEF1*), effector T cells (*TBX21* and *PRDM1*), and type-1 interferon response (*IRF7*) from RNA-seq.